Progress In Electromagnetics Research, Vol. 138, 389–405, 2013

FIVE-ZONE PROPAGATION MODEL FOR LARGE-SIZE VEHICLES INSIDE TUNNELS

Ke Guan[1], Zhangdui Zhong[1], Bo Ai[1, *], Ruisi He[1], and Cesar Briso-Rodríguez[2]

[1]State Key Laboratory of Rail Traffic Control and Safety, Beijing Jiaotong University, Beijing 100044, China

[2]Escuela Universitaria de Ingenierîa Técnica de Telecomunicación, Universidad Politécnica de Madrid, Madrid 28031, Spain

Abstract—An accurate characterization of the wave propagation inside tunnels is of practical importance for the design of advanced communication systems. This paper presents a five-zone propagation model for large-size vehicles inside tunnels. Compared with existing models, the proposed model considers the influence of the large size of the vehicle, and covers all propagation mechanism zones and their dividing points. When a large-size vehicle is passing the transmitter, the received power suffers a deep fading as the direct wave is blocked by the vehicle itself. This zone is called the near shadowing zone. Then, when the vehicle has moved past the transmitter, the line of sight is recovered. If the vehicle is still close to the transmitter, the free space propagation zone starts. Then, as the distance increases, the vehicle enters the multi-mode propagation zone, where higher order modes are significant. Further away, when high order modes are greatly attenuated, guided propagation is stabilized. Finally, when the vehicle is extremely far from the transmitter, the waveguide effect vanishes because of the attenuation of reflected rays. Two sets of measurements are employed to validate the model. Results show good agreement, and therefore, the model presents an effective way to predict the propagation inside tunnels for large-size vehicles.

Received 1 January 2013, Accepted 15 March 2013, Scheduled 28 March 2013

* Corresponding author: Bo Ai (myecone@hotmail.com).

1. INTRODUCTION

In order to respond to the growing demand for high-performance radio communication systems in complex environments, a number of contributions have been made to predict the propagation characteristics in the last decades [1–12]. As one of the most common environments, a tunnel can generate various specific mechanisms when the electromagnetic wave propagates inside it. In order to clarify these propagation mechanisms, based on different methods (e.g., in [5], etc.), more and more researchers are inclined to analyze the propagation characteristics by separating various zones along the tunnel. In order to describe the propagation characteristics inside tunnels, a number of models have been presented in a two slope curve [1] where the path loss is predicted by two different expressions with a different slope parameter. They indicate that there is a "critical distance" [5], usually called a break point [5]. The region before the break point is the near region, where high order modes are significant; guided propagation has not been well established, and therefore, the signal suffers higher loss. The region after the break point is the far region, where high order modes are highly attenuated; guided propagation is stabilized and undergoes lower loss.

Unfortunately, the viewpoints on the propagation mechanism in the near region are not uniform. Some dissertations are inclined to interpret the propagation before the break point with the single ray (free space) theory [7], others contend that it should be described by the multi-mode waveguide model [5]. However, a big amount of evidence proves that the free space mechanism sets up first, whereas multi-mode propagation mechanism comes later into play. Thus, it is desirable to redefine the propagation zones in the near region. Authors in [10] divide this region into two and model the path loss in both areas. For their dividing point, they employ the free-space model to calculate the location. This has been proved to be reasonable, but its validity requires certain conditions.

It is acknowledged that the propagation characteristics in the far region follow the fundamental-mode waveguide mechanism [5, 7, 10]; nevertheless, in some long tunnels, such as the road tunnel between Slovenia and Austria in [10], the waveguide effect is found to vanish at extremely long distances. This means a single far region cannot account for all the propagation mechanisms at long distances.

In most realistic vehicular communication cases, for vehicles the cross-section of which is comparable to the cross section of the tunnel and, at the same time, the length of which, although being smaller, has the same order of magnitude as the tunnel length, an important

phenomenon named near shadowing effect occurs. This is the case with trains in subway tunnels. When the large-size vehicle is in front of the transmitter (Tx), the signal power of receiver (Rx) suffers strong attenuation because the first Fresnel zone is blocked by the vehicle itself to some extent [13]. Such effect can be observed in a range of distances, and the propagation characteristics have to be identified as well.

In summary, the existing propagation models are neither complete nor unified. The influence of the large size (of the vehicle) has generally not been considered. This reduces the accuracy of radio planning and simulation for communication systems by a large extent. In order to overcome this limitation, a propagation model for large-size vehicles inside tunnels is presented herewith. This model interprets all propagation mechanisms for the large-size vehicles, and therefore, it can be useful to grasp the essence of the propagation and make accurate coverage prediction.

2. MODEL FOR LARGE-SIZE VEHICLES

The model is presented having in mind the large size of the vehicle, based on the change law of the propagation mechanisms along the tunnel. The model consists of five propagation zones, namely: the near shadowing zone (NSZ), the free space propagation zone (FSPZ), the multi-mode propagation zone (MMPZ), the fundamental model propagation zone (FMPZ), and the extreme far zone (EFZ). As shown in Figure 1, the model is more comprehensive than the existing models. Whether the free space propagation zone can exist depends on the length of the large-size vehicle. If the large-size vehicle is so long that the near shadowing zone is longer than the free space propagation zone, no free space mechanism will be observed. If the vehicle is so short that the Rx can still be near the Tx when the near shadowing zone is finished, the free space propagation zone will come after.

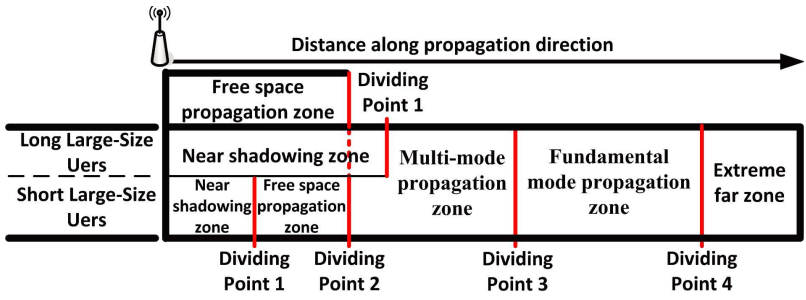

Figure 1. Propagation model for large-vehicles inside tunnels.

Compared with the traditional two-slope model [1], the five-zone model subdivides the near region into the free space propagation zone and the multi-mode propagation zone. This clearly reveals the mechanism structure in the previously so-called near region [5]. Moreover, the presented model adds the extreme far zone so that the fact that the waveguide effect vanishes at extreme distances is identified. Compared with the advanced four-slope model [10], the five-zone model strengthens the algorithm of the dividing points and finally deduces the analytical solution of the location of dividing points inside arbitrary cross-sectional tunnels. Furthermore, the supplement of the near shadowing zone depicts the near shadowing phenomenon of the large-size vehicles, which can be valuable for the design of radio telecommunication systems in realistic subway tunnels.

Since single modeling technique is always sensitive to certain propagation mechanism, a hybrid propagation model integrating advantages of different techniques is considered in this investigation. In the free space propagation zone and the extreme far zone, the channel loss is modeled by the free space loss. In the near shadowing zone, path loss and shadow fading are the most primary factors, thus a statistical model is utilized here. In the multi-mode propagation zone and the fundamental model propagation zone, an enhanced multi-mode model is proposed by improving the modal analysis and transforming the advantages of ray tracing methods [14]. Since there is an interaction between the path loss curves in different zones, the continuity of the predicted path loss can be ensured in the transition between two zones.

2.1. Statistical Modeling in Near Shadowing Zone

This zone is discovered in the measurements reported in [13]. In the measurements, transmitters are installed at 4 m above the floor; 25 cm from the tunnel walls; with operating frequencies at 2400 MHz. The transmitter covers the 2.4/2.5-GHz band with an output power of 20 dBm. It has a 3-dB power splitter to feed two HyperLink HG2409P antennas (circular polarization with 8-dBi gain), each one pointing to one side of the tunnel.

The receiving antennas are the same as for the transmitters but vertical polarized with 65° horizontal and vertical beam width. The measurements employed a configuration of two antennas, one installed in the front and one in the rear car of the train, 2.2 m from the nearest wall and 4.5 m above the track. The receiver is a spectrum analyzer with a preamplifier and a power splitter to connect the two antennas located on the train. This configuration is known to provide good diversity, and therefore, it is widely used in subways.

In this set of measurements, the near shadowing effect has been

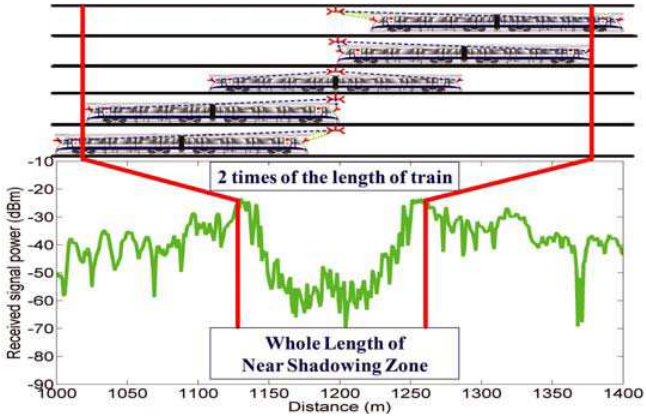

Figure 2. Sketch of the process of the near shadowing zone.

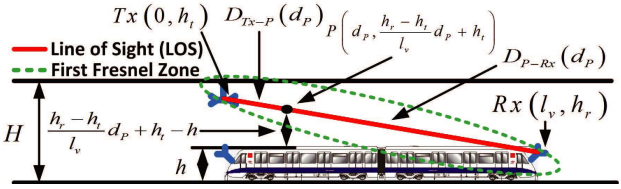

Figure 3. Sketch of the mechanism of near shadowing phenomenon.

observed: when the train is in front of the Tx, the received power suffers a deep fading and propagation is definitely multi-path. Figure 2 demonstrates the whole process of the near shadowing phenomenon. Such effect occurs when the first Fresnel zone, especially the 60% of the first Fresnel zone is blocked by the vehicle. Hence, as shown in Figure 3, the critical condition can be given when the vertical distance between any point P on the line of sight (LOS) and the top of the vehicle is equal to the 60% of the radius of the first Fresnel zone:

$$\frac{h_r - h_t}{l_v} d_p + h_t - h = \frac{60}{100} \sqrt{\frac{\lambda D_{\mathrm{Tx}-P}(d_P)\, D_{P-\mathrm{Rx}}(d_P)}{D_{\mathrm{Tx}-P}(d_P) + D_{P-\mathrm{Rx}}(d_P)}} \tag{1}$$

By substituting $d_P = \frac{l_v}{2}$ into (1), the equation can be written as $h_t + h_r - 2h = 0.6\sqrt{\lambda l_v}$, which means even the widest part of the first Fresnel zone (the Maximum Fresnel zone plate) is touched by the vehicle. As in practice the transmitting antenna is normally installed near the top of the tunnel, and the receiving antenna is mounted on the vehicle, the following approximations can be allowed: $h_t \approx H$, $h_r \approx h$.

So, the critical condition can be simplified as:

$$H - h = 0.6\sqrt{\lambda l_v} \tag{2}$$

where H and h denote the height of the tunnel and vehicle, respectively. λ denotes the wavelength. l_v denotes the length of the vehicle. This simplified equation can be used as a rough criterion to judge the existence of the near shadowing phenomenon. When $H-h < 0.6\sqrt{\lambda l_v}$, the near shadowing phenomenon should be considered; when $H - h > 0.6\sqrt{\lambda l_v}$, no near shadowing phenomenon occurs.

Figure 4(a) shows the measured received power when the train is in the subway tunnel at 2.4 GHz [13]. In this measurement, $(H - h = 0.8) < (0.6\sqrt{\lambda l_v} = 1.64)$. Thus, the near shadowing phenomenon can be clearly observed. Figure 4(b) shows the received power when the train is in the high-speed railway tunnel at 900 MHz [5]. In this case, $(H - h = 2.8) > (0.6\sqrt{\lambda l_v} = 2.68)$. Hence, the near shadowing zone does not exist.

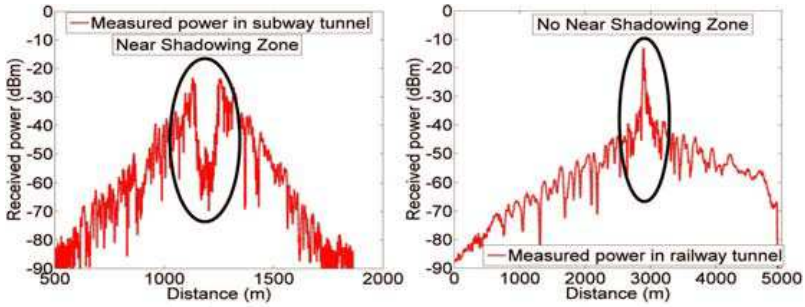

Figure 4. Measured received power when the train is (a) in the narrow subway tunnel (4.8 m × 5.3 m) at 2.4 GHz [13], and (b) in the large high-speed railway tunnel (10.7 m × 6.3 m) at 900 MHz [5].

Denote the maximum near shadowing loss when there is no LOS between the Tx and the Rx by $NL_{\max}$. Since such non-LOS situation results from the block effect of the carriage, following relation holds: the bigger the train, the more easily the LOS is blocked; the bigger the tunnel, the harder LOS is blocked. Thus, $NL_{\max}$ is proportional to the height and width of the section of the train, but inversely proportional to the height and width of the section of the tunnel. With this analysis, by using the principle of least-squares curve fitting on the measured data in [13], $NL_{\max}$ can be modeled as:

$$NL_{\max} = 16.1 \times \frac{h}{H} + 31.2 \times \frac{w}{W} \tag{3}$$

where w and h denote the width and height of the train, respectively; W and H denote the width and height of the tunnel, respectively.

By using the point slope form, the propagation loss $L_{R_{NS}}$ in the near shadowing zone is expressed by

$$L_{R_{NS}} = \frac{PL_l - (NL_{\max} + PL_0)}{l_{\text{near}}} |z_r - z_t| + (NL_{\max} + PL_0) + X_\sigma \quad (4)$$

where $|z_r - z_t|$ denotes the distance between Tx and Rx; PL_l denotes the path loss at the point where the distance is the length of the vehicle (i.e., train); l_{near} denotes the half length of the near shadowing zone, always equaling the length of the vehicle; PL_0 denotes the path loss under LOS condition when the distance between the vehicle and the Tx is 0 m, which can be calculated by the free space model. X_σ represents a log-normal distribution with standard deviation σ [13].

2.2. Propagation Loss in the Free Space Propagation Zone

When the near shadowing zone is finished and the Rx is still near the Tx, the propagation characteristics can follow the rule of free space propagation. This region is thus named as the "free space propagation zone". Similarly naming method is used in [10], where such zone is reported as the free space segment. In this zone, the angles of incidence from the rays to the walls are high resulting in high attenuation of reflected rays, whereas the path difference between direct and reflected rays may also cause additional attenuation, so only the direct ray significantly contributes to the strength of the received signal. The channel loss in this segment follows the free space loss.

$$PL \text{ (dB)} = -10 \log_{10} \left[\frac{\lambda^2}{(4\pi)^2 |z_r - z_t|^2} \right] \quad (5)$$

2.3. Enhanced Multi-mode Modeling in the Multi-mode Propagation Zone and Fundamental Model Propagation Zone

To predict the propagation in the multi-mode propagation zone and the fundamental model propagation zone, an enhanced multi-mode model is proposed. Compared with [15], the proposed model clarifies the limitation of the modes and introduces new calibrating factors.

If the cross-section of the cylindrical tunnel is, for modeling purposes, replaced by an equivalent rectangle, then modal theory can be used and the tunnel is regarded as an oversized hollow rectangular waveguide. In modal theory, propagation in tunnels is represented by the superposition of multiple modes. Hence, by deducing the field of

each mode and introducing two modifying factors (the tilt loss L_{tilt} and the roughness loss $L_{\text{roughness}}$) [16], the propagation loss $L_{R_{MW}}$ at the coordinate $(x,\, y,\, |z_r - z_t|)$ is given by:

$$\begin{aligned} L_{R_{MW}} \;=\; & L_{\text{tilt}}\left(|z_r - z_t|\right)\,[\text{dB}] + L_{\text{roughness}}\left(|z_r - z_t|\right)\,[\text{dB}] \\ & -20\lg\left(\frac{1}{E_0}E^{\text{Rx}}\left(x, y, |z_r - z_t|\right)\right) - G_t\,[\text{dB}] - G_r\,[\text{dB}] \end{aligned} \quad (6)$$

where E^{Rx} is the field strength in the rectangular tunnel, which has been derived in [15]. E_0 is the field at the transmitter; G_t and G_r are the antenna gains of the transmitter and the receiver, respectively.

2.4. Propagation Loss in the Extreme Far Zone

When the distance between the Tx and the Rx is extremely large, the waveguide effect vanishes because of the attenuation at each reflection, so the path loss slope obeys the free space propagation loss curve, with occasional deep fades due to a single reflected ray from the walls of the tunnel. This propagation zone is observed both in [5, 10].

Note that this propagation zone is usually not relevant to those cellular communication systems, where the cell radius is shorter than 500 m, as the cell boundary is reached and handover occurs before the base station-to-mobile terminal distance reaches the "extremely far zone" value. However, this zone can not be ignored in public protection and disaster relief communications.

3. MODELING FOR DIVIDING POINT (DV)

3.1. Modeling for Dividing Point 1

As shown in Figure 2, when the distance between the vehicle (train) and Tx is shorter than the length of the vehicle (train), the signal is blocked by the carriage so that the near shadowing effect occurs. When the vehicle (train) is running out of this region, the coverage recovers. The length of the near shadowing region is two times the length of the vehicle (train) (in [13] is $(2 \times 60\,\text{m})$). In fact, this phenomenon exists when (2) is fulfilled. Thus, the distance between the Dividing Point 1 and the Tx is the length of the vehicle:

$$z_{\text{DV}}^{\text{NSZ-MMZ}} = l_v \quad (7)$$

3.2. Modeling for Dividing Point 2

According to the geometry, it is easy to determine the distance between the tangent line/curve (of the Maximum Fresnel zone plate and the

walls) and the middle point (of the LOS between Tx and Rx). If this distance is larger than the radius of the Maximum first Fresnel zone plate, the first Fresnel zone can be treated as almost clear. Thus, the relative relation between this distance and the radius can be employed to reflect the interaction between the first Fresnel zone and the walls.

Figure 5 depicts the schematic diagram of an arbitrary cross-sectional tunnel, Tx, Rx, LOS, and the Maximum first Fresnel zone.

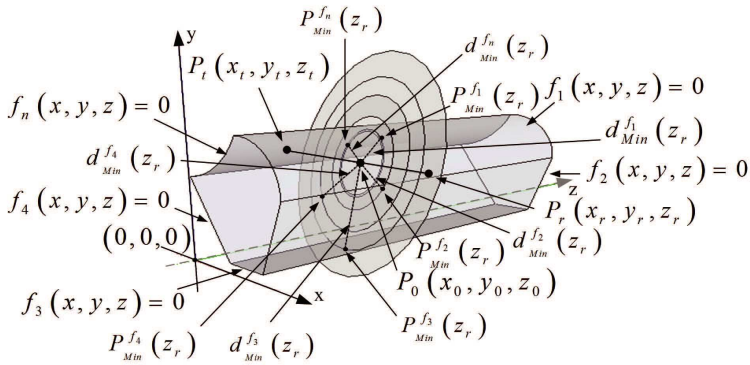

Figure 5. Detailed schematic diagram of the propagation inside arbitrary cross-sectional tunnels with the first Fresnel zone clearance.

According to the three-dimensional solid geometry, the arbitrary cross-sectional tunnel consists of a set of plane surfaces and curved surfaces whose coordinates x, y, z satisfy the following equation

$$f_i(x, y, z) = 0, \quad i = 1, 2, \ldots, n \tag{8}$$

The coordinates of Tx, Rx, and the middle point on the LOS between Tx and Rx are $P_t(x_t, y_t, z_t)$, $P_r(x_r, y_r, z_r)$, and $P_0(x_0, y_0, z_0)$. Then, the intersection between the Maximum Fresnel zone plane and the surface f_i of the tunnel is a curve or a line that can be given by

$$\begin{cases} (x_r - x_t)\left(x - \frac{x_r + x_t}{2}\right) + (y_r - y_t)\left(y - \frac{y_r + y_t}{2}\right) \\ + (z_r - z_t)\left(z - \frac{z_r + z_t}{2}\right) = 0 \\ f_i(x, y, z) = 0, \quad i = 1, 2, \ldots, n \end{cases} \tag{9}$$

Define the first equation as a function $g(x, y, z)$; define the second equation as a function $f_i(x, y, z)$.

In order to find the minimum distance between the intersection (line/curve) and the middle point $P_0(x_0, y_0, z_0)$ on the LOS, the Lagrange multiplier method is employed. Construct a function:

$$F_i(x, y, z, \rho_i, \lambda_i) = \left(x - \frac{x_r + x_t}{2}\right)^2 + \left(y - \frac{y_r + y_t}{2}\right)^2$$

$$+\left(z-\frac{z_r+z_t}{2}\right)^2+\rho_i\cdot g(x,y,z)+\lambda_i\cdot f_i\,(x,y,z) \tag{10}$$

where ξ, μ are the lagrange multipliers. By equating to zero the partial derivatives of F_i with respect to x, y, and z and to the Lagrange multipliers, the coordinates of the intersection point at the minimum distance to $P_0(x_0, y_0, z_0)$ can be obtained: $p_{\min}^{f_i}(x^{f_i}(z_r), y^{f_i}(z_r), z^{f_i}(z_r))$. Thus, the minimal distance between P_0 and the intersection between the Maximum Fresnel zone plane and the surface f_i can be expressed as

$$\begin{aligned} d_{\min}^{f_i}(z_r) \;=\; & \left[\left(x^{f_i}(z_r)-\frac{x_r+x_t}{2}\right)^2+\left(y^{f_i}(z_r)-\frac{y_r+y_t}{2}\right)^2\right. \\ & \left.+\left(z^{f_i}(z_r)-\frac{z_r+z_t}{2}\right)^2\right]^{\frac{1}{2}} \end{aligned} \tag{11}$$

The maximum radius of the first Fresnel zone is determined by

$$r_{1\max}(z_r)=\frac{1}{2}\sqrt{\lambda d_{P_tP_r}} \tag{12}$$

where $d_{P_tP_r}$ denotes the distance between the Tx and the Rx. The propagation theory indicates that the free space model can be applied if the first Fresnel zone is free of any obstacles. Therefore, if only the wall $f_i(x, y, z)$ could be touched by the Maximum first Fresnel zone, the dividing point between two propagation mechanisms locates at ${z_r}_{\min}^{f_i}$ that is the minimal positive real root of the following equation

$$r_{1\max}(z_r)=d_{\min}^{f_i}(z_r) \tag{13}$$

In fact, there are totally n walls of the arbitrary cross-sectional tunnels that could be tangent to the Maximum first Fresnel zone. Therefore, the Dividing Point 1 locates at $z_{\mathrm{DV}}^{\mathrm{FSZ-MMZ}}$ when the Maximum first Fresnel zone first touches any one of the walls:

$$z_{\mathrm{DV}}^{\mathrm{FSZ-MMZ}}=\min\left\{z_{r\min}^{f_i},\, i=1,2,\ldots,n\right\} \tag{14}$$

3.3. Modeling for Dividing Point 3

The Dividing Point 3 is called the "break point" by a number of propagation models inside tunnels [5]. By assuming an equivalent rectangular tunnel, the location of the Dividing Point 3 is defined as the distance where the second-order modes have suffered one reflection

from vertical or horizontal walls. By using the basic model in [5], the distance from the Tx to the break point can be given by:

$$z_{\mathrm{DV}}^{\mathrm{MMZ-FMZ}} \approx \max\left(\frac{W^2}{\lambda}, \frac{H^2}{\lambda}\right) \tag{15}$$

where $z_{\mathrm{DV}}^{\mathrm{MMZ-FMZ}}$ is the location of the Dividing Point 3; W, H are the width and height of the equivalent rectangular tunnel, respectively.

3.4. Modeling for Dividing Point 4

The Dividing Point 4 indicates the extinction of the wave guide mechanism. Thus, it can be defined as the distance where the fundamental modes E_{11}^h (horizontally polarized E-field) and E_{11}^v (vertically polarized E-field) have suffered one reflection. In the ray theory, the E_{11}^h and E_{11}^v modes are both defined by the phase relations:

$$\sin\phi_1 = \frac{\lambda}{2W} \quad \sin\phi_2 = \frac{\lambda}{2H} \tag{16}$$

where ϕ_1 and ϕ_2 are the grazing angles of incidence of the rays with the vertical and horizontal walls, respectively. When the wavelength λ is small in comparison with W and H, the sine can be approximated by its tangent. As shown in the Figure 6, the distance z_{DV}^v where the E_{11}^v has suffered one reflection from vertical walls is given by:

$$z_{\mathrm{DV}}^v \approx \frac{[\max(y_t, H - y_t)]^2}{\lambda} + \frac{[\max(y_r, H - y_r)]^2}{\lambda} \tag{17}$$

where y_t and y_r are the vertical coordinates of Tx and Rx, respectively. Correspondingly, the distance in horizontal direction z_{DV}^h is given by

$$z_{\mathrm{DV}}^h \approx \frac{[\max(x_t, W - x_t)]^2}{\lambda} + \frac{[\max(x_r, W - x_r)]^2}{\lambda} \tag{18}$$

where x_t and x_r are the horizontal coordinates of Tx and Rx, respectively. Finally, the location of the Dividing Point 4 ($z_{\mathrm{DV}}^{\mathrm{MMZ-FMZ}}$)

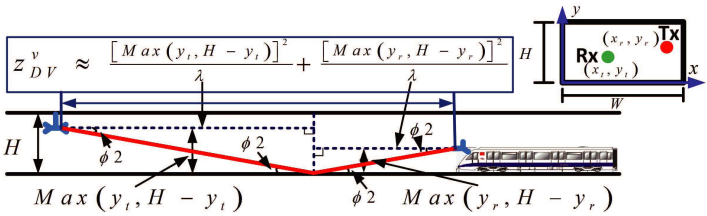

Figure 6. The vertical fundamental mode suffers one reflection.

is given by considering vertical and horizontal walls:

$$z_{\mathrm{DV}}^{\mathrm{FMZ-EFZ}} \approx \max\left(z_{\mathrm{DV}}^{v}, z_{\mathrm{DV}}^{h}\right) \tag{19}$$

3.5. Summary of the Localizations of the Dividing Points

The locations of the four dividing points are summarized as follows:

- Dividing Point 1: Figure 3 and the critical condition (2) indicate that the existence of the near shadowing phenomenon depends on the frequency, and sizes of the vehicle and the tunnel. When the inequation $H - h < 0.6\sqrt{\lambda l_v}$ holds and the near shadowing effect occurs, the location of the Dividing Point 1 mainly depends on the size of the vehicle.
- Dividing Point 2: It does not obviously depend on the size of the vehicle, but is determined by the distance when the Maximum first Fresnel zone first touches any one of the walls.
- Dividing Point 3: It locates at the distance where the second-order modes have suffered one reflection from vertical or horizontal walls. Equation (15) clearly shows the law how the size of the tunnel determines the location of the Dividing Point 3.
- Dividing Point 4: It locates at the distance where the fundamental modes have suffered one reflection from walls. It depends on the frequency, the size of tunnel, and the locations of the Tx and Rx.

4. SIMULATION AND MODEL VALIDATION

To validate the five-zone model, two sets of measurements have been employed. The first set of measurements are performed at 2.4 GHz, for the planning of the CBTC system in the Line 10 tunnels of Madrid's subway [13]. According to the test system configuration and environment, following parameters are used in the simulation: $f_0 = 2.4 \times 10^9$, $\lambda = 0.125$, $W = 4.8$, $H = 5.3$, $x_t = 0.25$, $y_t = 4$, $z_t = 0$, $x_r = 4$, $y_r = 3.5$, $\theta = 0.22$, $\gamma = 0.2$, $\varepsilon_v = 5$, $\varepsilon_h = 5$, $\varepsilon_a = 1$, $\sigma_v = 0.01$, $\sigma_h = 0.01$, $\sigma_a = 0$, $\mu_0 = 4\pi \times 10^{-7}$, $\varepsilon_0 = 8.85 \times 10^{-12}$, where f_0 denotes the central frequency of the signal; ε_v, ε_h, and ε_a are the relative permittivity for vertical/horizontal walls and the air in the tunnel, respectively. σ_v, σ_h, and σ_a are the conductivity for vertical/horizontal walls and the air in the tunnel, respectively. μ_0 denotes the permeability for vertical/horizontal walls and the air in the tunnel. ε_0 is the permittivity in vacuum space. θ and γ are the root-mean-square tilt and roughness of the tunnel walls, respectively.

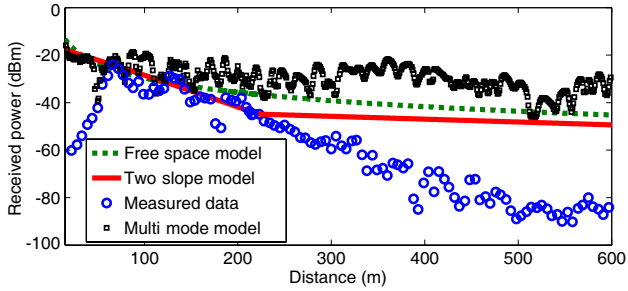

Figure 7. Comparisons between measurement in subway tunnel (4.8 m × 5.3 m) at 2.4 GHz and the existing models.

Figure 7 shows comparisons between measurements in subway and the free space model, traditional two-slope model (e.g., in [5]), and multi-mode model (e.g., in [15]). Large difference can be observed. This deviation mainly comes from the neglect of the near shadowing effect and the extra loss due to wall tilt and roughness. These two features have been included into the five-zone model.

The second group of measurements are carried out in the tunnels on the new high-speed train line from Madrid to Lleida in Spain [5], with the following parameters: $f_0 = 900 \times 10^6$, $W = 10.7$, $H = 6.3$, $x_t = 11.43$, $y_t = 3$, $z_t = 0$, $x_r = 8.43$, $y_r = 3$, $\theta = 0.1$, $\gamma = 0.12$, $\varepsilon_v = 5$, $\varepsilon_h = 5$, $\varepsilon_a = 1$, $\sigma_v = 0.01$, $\sigma_h = 0.01$, $\sigma_a = 0$, $\mu_0 = 4\pi \times 10^{-7}$, $\varepsilon_0 = 8.85 \times 10^{-12}$, and the curvature radius of the roof $R = 6.2$.

As shown in Figure 8, the predicted result of the proposed model and the measured received power in the both subway tunnel and the railway tunnel have good agreement in every propagation zone. The mean (Mean Error), standard deviation (Std), and root mean square (RMSE) of the difference are summarized in Table 1. The proposed model has a 0–2 dB Mean Error and 4.59–6.18 dB Std, better than existing models that have large deviations shown in Figure 7.

Note that in the case of the subway tunnel at 2.4 GHz shown in Figure 8(a), the free space propagation zone and the extreme far zone do not show up. This is because the length of the near shadowing zone (which is twice of the length of the train) is greater than the free space propagation zone (calculated by the model), so the free space propagation zone is replaced by the near shadowing zone, and the Dividing Point 2 does not exist. The attenuation at 2.4 GHz is high and the received power is below the reception threshold before the distance extends to the extreme far zone. So, the extreme far zone and the Dividing Point 4 cannot be observed. The features not observed in the case of Figure 8(a) are, instead, clearly seen in the case of the

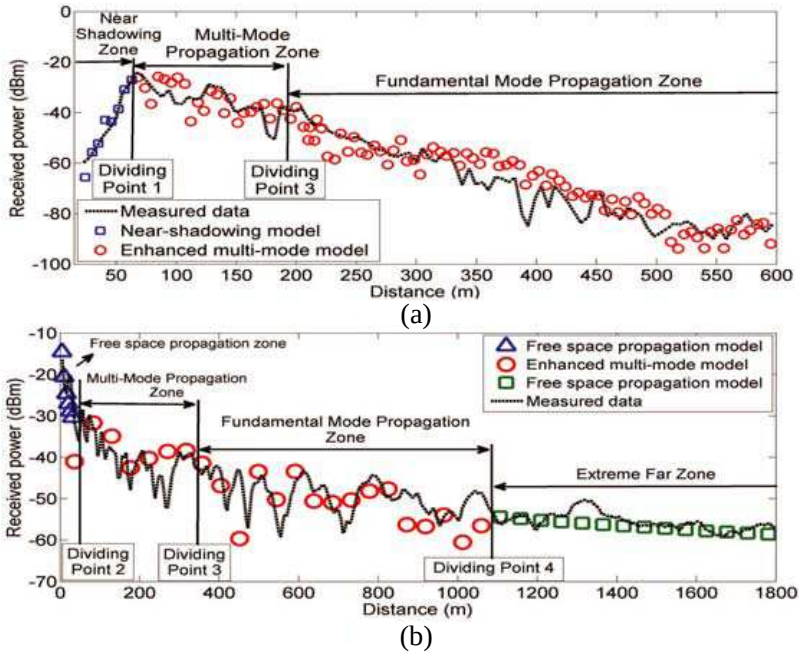

Figure 8. Comparisons between proposed model and measurements (a) subway tunnel (4.8 m × 5.3 m) at 2.4 GHz and (b) railway tunnel (10.7 m × 6.3 m) at 900 MHz.

Table 1. Mean, standard deviation, and root mean square of the difference (measurement vs. proposed propagation model).

Measurement in narrow subway tunnel (4.8 m × 5.3 m) at 2.4 GHz

Statistics	NSZ	FSPZ	MMPZ	FMPZ	EFZ	Whole Model
Mean Error (dB)	1.46	-	0.02	2.14	-	1.48
Std (dB)	4.61	-	5.37	6.49	-	6.18

Measurement in large railway tunnel (10.7 m × 6.3 m) at 900 MHz

Statistics	NSZ	FSPZ	MMPZ	FMPZ	EFZ	Whole Model
Mean Error (dB)	-	0.91	3.03	1.54	1.26	0.72
Std (dB)	-	3.89	3.61	5.97	1.6	4.59

railway tunnel at 900 MHz shown in Figure 8(b). Since the railway tunnel is very large, the LOS will not be blocked even when the train is passing the transmitter. Thus, the near shadowing zone and the Dividing Point 1 do not exist in this case.

The model for the dividing points have been validated by several groups of measurement campaigns in [1, 5, 10, 13]. The chosen measurements are with different types and shapes of tunnels at different frequencies. Comparison results are given in Table 2.

Table 2. Comparisons of DV between model and measurements.

DV	Tunnel	Frequency (GHz)	Measurement	Prediction
1	Subway tunnel [13]	2.4	60.5–65 m	60 m
2	Vehicle tunnel [1]	0.45	35–40 m	37.88 m
2	Railway tunnel [5]	0.9	30–35 m	30.86 m
2	Road tunnel [10]	0.4	15 m	15.41 m
3	Railway tunnel [5]	0.9	327–357 m	347 m
3	Subway tunnel [13]	2.4	182–204 m	184.3 m
4	Railway tunnel [5]	0.9	1100–1200 m	1101 m
4	Road tunnel [10]	0.4	1200–1312 m	1240 m

5. CONCLUSION

This paper presents a five-zone propagation model for large-size vehicles. This model covers all possible propagation mechanisms, corresponding regions, and propagation characteristics when a large-size vehicle is inside tunnels, refining and extending existing models. By substituting parameters, the model can be used to accurately simulate radio propagation in tunnels. The analysis, modeling, and results in this paper are helpful to gain deeper insight and better understanding of electromagnetic propagation inside tunnels.

ACKNOWLEDGMENT

This paper was sponsored by the NNSF of China under Grant 61222105, Beijing NSF 4112048, 2010JBZ008, RCS2011ZZ008, RCS2010K008, the Program for Changjiang Scholars and Innovative Research Team in University under Grant No. IRT0949, the Key Grant Project of Chinese Ministry of Education (No. 313006), and the Spanish National R & D project Tecrail IPT-2011-1034-370000. We thank the anonymous reviewers for their constructive comments, which greatly helped to improve the paper.

REFERENCES

1. Dudley, D. G., M. Lienar, S. F. Mahmud, and P. Degauque, "Wireless propagation in tunnels," *IEEE Antennas Propag. Magazine*, Vol. 49, 11–26, 2007.
2. Phaebua, K., C. Phongcharoenpanich, M. Krairiksh, and T. Lertwiriyaprapa, "Path-loss prediction of radio wave propagation in an orchard by using modified UTD method," *Progress In Electromagnetics Research*, Vol. 128, 347–363, 2012.
3. Yu, X., L. Wang, H.-G. Wang, X. Wu, and Y.-H. Shang, "A novel multiport matching method for maximum capacity of an indoor MIMO system," *Progress In Electromagnetics Research*, Vol. 130, 67–84, 2012.
4. Soria, G. A. S., J. M. Riera, P. Garcia del Pino, and J. Romeu, "Atmospheric propagation at 100 and 300 GHz: Assessment of a method to identify rainy conditions during radiosoundings," *Progress In Electromagnetics Research*, Vol. 130, 257–279, 2012.
5. Briso-Rodriguez, C., J. M. Cruz, and J. I. Alonso, "Measurements and modeling of distributed antenna systems in railway tunnels," *IEEE Trans. Veh. Technol.*, Vol. 56, 2870–2879, 2007.
6. Taha-Ahmed, B., D. F. Campillo, and J. L. Masa-Campos, "Short range propagation model for a very wideband directive channel at 5.5 GHz band," *Progress In Electromagnetics Research*, Vol. 130, 319–346, 2012.
7. Zhang, Y. P., "Novel model for propagation loss prediction in tunnels," *IEEE Trans. Veh. Technol.*, Vol. 52, 1308–1314, 2003.
8. Tao, R., L. Si, Y. Ma, P. Zhou, and Z. Liu, "Relay propagation of partially coherent cosh-Gaussian beams in non-Kolmogorov turbulence," *Progress In Electromagnetics Research*, Vol. 131, 495–515, 2012.
9. Harun, A., D. L. Ndzi, M. F. Ramli, A. Y. M. Shakaff, M. N. Ahmad, L. M. Kamarudin, A. Zakaria, and Y. Yang, "Signal propagation in aquaculture environment for wireless sensor network applications," *Progress In Electromagnetics Research*, Vol. 131, 477–494, 2012.
10. Hrovat, A., G. Kandus, and T. Javornik, "Four-slope channel model for path loss prediction in tunnels at 400 MHz," *IET Microwaves, Antennas and Propagation*, Vol. 4, 571–582, 2010.
11. Zhang, Y., W. Zhai, X. Zhang, X. Shi, X. Gu, and Y. Deng, "Ground moving train imaging by Ku-band radar with two receiving channels," *Progress In Electromagnetics Research*, Vol. 130, 493–512, 2012.

12. Li, B., Z. Zhou, D. Li, and S. Zhai, "Efficient cluster identification for measured ultra-wideband channel impulse response in vehicle cabin," *Progress In Electromagnetics Research*, Vol. 117, 121–147, 2011.
13. Guan, K., Z. D. Zhong, B. Ai, C. Briso, and J. I. Alonso, "Measurement of distributed antenna systems at 2.4 GHz in a realistic subway tunnel environment," *IEEE Trans. Veh. Technol.*, Vol. 61, 834–837, 2012.
14. Liu, Z.-Y. and L.-X. Guo, "A quasi three-dimensional ray tracing method based on the virtual source tree in urban microcellular environments," *Progress In Electromagnetics Research*, Vol. 118, 397–414, 2011.
15. Sun, Z. and I. F. Akyildiz, "Channel modeling and analysis for wireless networks in underground mines and road tunnels," *IEEE Trans. on Communications*, Vol. 58, No. 6, 1758–1768, 2010.
16. Emslie, A. G., R. L. Lagace, and P. F. Strong, "Theory of the propagation of UHF radio waves in coal mine tunnels," *IEEE Trans. Antennas Propag.*, Vol. 23, No. 2, 192–205, 1975.